Structural Analysis of a Cs + O Coadsorption Phase on a Ru(0001) Surface

M. Gierer, H. Bludau, H. Over, and G. Ertl

Abteilung Physikalische Chemie, Fritz-Haber-Institut der Max-Planck-Gesellschaft, Faradayweg 4–6, D-14195 Berlin

Z. Naturforsch. **50a**, 453–458 (1995); received September 15, 1994

Dedicated to Professor Dr. E. Wicke on the occasion of his 80th birthday

The adsorption of oxygen onto a Ru(0001)–(2 × 2)–Cs phase with coverage $\Theta_{Cs} = 0.25$ gives rise to the formation of a Ru(0001)–$(2\sqrt{3} \times 2\sqrt{3})$R 30°–3Cs–2O coadsorption structure with three cesium and two oxygen adatoms in the unit cell. A low-energy electron-diffraction (LEED) analysis reveals that oxygen is located in threefold hollow sites on the Ru surface while the Cs atoms remain near on-top sites; this site was also found in the pure Ru(0001)–(2 × 2)–Cs phase. The oxygen–Ru bond length of (2.14 ± 0.05) Å is longer by 0.11 Å than in the Ru(0001)–(2 × 2)–O phase, indicating that the Ru–O bond is weakened in the presence of coadsorbed Cs. The Cs hard sphere radius of (1.75 ± 0.07) Å is close to the ionic Pauling radius of 1.69 Å.

1. Introduction

The properties of cesium and oxygen adsorbed on Ru(0001) have been the subject of several investigations (see, e.g., [1]), not only because of fundamental interest, but also for the role such layers play as electronic promoters in catalytic reactions such as ammonia synthesis [2]. While thick Cs layers on a Ru(0001) surface after oxidation reflect the chemistry of Cs oxide bulk materials [3], in the submonolayer regime the interactions of Cs and O with the Ru substrate come additionally into play and may prevent the formation of bulk-like Cs oxides. In contrast to thick Cs films, in the submonolayer range the presence of a large variety of ordered phases depending on the Cs and O coverage [4] makes it possible to obtain structural information using LEED and, hence, to gain deeper insight into the Cs–O surface chemistry and the interactions between the adsorbates and the substrate. One of these phases, namely the Ru(0001)–$(\sqrt{3} \times \sqrt{3})$R 30°–Cs–O structure, has already been the subject of a LEED structural analysis [5]. Starting with an ordered Ru(0001)–$(\sqrt{3} \times \sqrt{3})$R 30°–Cs structure with Cs coverage $\Theta_{Cs} = 0.33$, addition of O_2 and subsequent annealing leads first to the formation of an incommensurate phase and with further oxygen exposure to the reappearance of a $(\sqrt{3} \times \sqrt{3})$R 30° structure with maximum intensity at a coverage ratio of $\Theta_{Cs}:\Theta_O = 1:1$. A LEED structure analysis revealed that both Cs and O atoms reside in threefold hcp sites. The Cs–Ru bond length is reduced by 0.08 Å compared with the $(\sqrt{3} \times \sqrt{3})$-Cs structure without oxygen [6], while the Ru–O bond length was determined to be 0.13 Å larger than in the Ru(0001)–(2 × 2)–O phase [7]. This effect was interpreted as being a consequence of charge transfer from the Cs to the more electronegative O adatoms.

At a Cs coverage of $\Theta_{Cs} = 0.25$, a (2 × 2)-phase shows up in which the Cs adatoms reside in on-top sites as evidenced by a LEED analysis [6]. Oxygen exposure to this phase at a sample temperature of $T = 310$ K leads among others to the formation of a $(2\sqrt{3} \times 2\sqrt{3})$R 30° phase with highest intensity of its superstructure spots after O_2 exposure of 0.3 L ($1\ L = 1.3 \times 10^{-6}$ mbar s) [4]. In this contribution, we report on a quantitative LEED analysis of this coadsorbate structure.

2. Experimental

The experiments were carried out in a UHV chamber equipped with facilities for thermal desorption spectroscopy (TDS) and Auger electron spectroscopy (AES). The LEED experiments were performed with a display-type four-grids optics and the integral spot intensities were measured using a computer-controlled video LEED system. Further details about the experimental setup can be found in [4, 6]. For the LEED structural analysis, 3 integer and 7 fractional-

Reprint requests to Dr. H. Over.

0932-0784 / 95 / 0400-0453 $ 06.00 © – Verlag der Zeitschrift für Naturforschung, D-72027 Tübingen

order beams were measured at normal incidence and a sample temperature of $T = 100$ K.

3. Results and Discussion

The oxygen coverage in the $(2\sqrt{3}\times 2\sqrt{3})$R 30° phase is $\Theta_O = 0.16$; it was determined by means of AES and calibrated by combined AES and LEED measurements of the (2×2) and (2×1) phase of the system Ru(0001)–O with coverages $\Theta_O = 0.25$ and 0.5, respectively. A striking feature of the LEED pattern of the $(2\sqrt{3}\times 2\sqrt{3})$R 30° structure is the high intensity of the half-order beams, if compared with the other superstructure spots, indicating that the (2×2)–Cs layer is only slightly distorted by the presence of oxygen. The number of Cs atoms in the unit cell of the $(2\sqrt{3}\times 2\sqrt{3})$R 30° structure is three, consistent with a distorted (2×2)–Cs layer. Assuming that oxygen is uniformly distributed over the surface, the $(2\sqrt{3}\times 2\sqrt{3})$R 30° unit cell contains two oxygen atoms. This assumption is justified by the fact that the onset of Cs desorption in the TD spectrum is shifted towards higher temperatures compared to the oxygen-free (2×2)–Cs structure, which is indicative of a well-mixed Cs–O structure where the Cs adatoms are stabilized by the adsorbed oxygen [4].

High-resolution electron energy loss (HREEL) spectra of a Ru(0001)–Cs–O coadsorption phase with $\Theta_{Cs} = 0.25$ after oxygen exposure of 0.3 L exhibited signals at 62 meV and 23 meV which were attributed to the Ru–O and Cs–O vibrations, respectively [8, 9]. Vibration losses typical for molecular oxygen could not be detected. One can therefore safely assume that oxygen is adsorbed atomically in the $(2\sqrt{3}\times 2\sqrt{3})$R 30° phase. A vibration loss at 7.8 meV assigned to the Cs–Ru stretching mode could be observed with the Ru(0001)–Cs system at low Cs coverage ($\Theta_{Cs} = 0.08$), but not at $\Theta_{Cs} = 0.25$ [8]. This effect was interpreted as being a consequence of the screening of the dipole fluctuations via the delocalized electrons provided by the Cs atoms. Oxygen adsorption on the Ru(0001) surface precovered with Cs at $\Theta_{Cs} = 0.25$ leads to a reionization of the Cs layer and the reappearance of the Cs–Ru loss, consistent with a charge transfer from cesium to oxygen.

Theoretical $I(E)$ curves were computed using the program package of W. Moritz with extensive exploitation of symmetry relations, both in real and reciprocal space [10]. In the LEED program up to 9 spin-averaged phase shifts were used which were calculated in the framework of the "muffin-tin" approximation [11] by solving the Dirac equation with Slater's exchange term and Schwarz's optimized α-parameter [12]. An important parameter determining the scattering potential of Cs is the muffin-tin-radius, which is roughly given by half the Cs–Cs nearest-neighbor distance when the Cs atoms are arranged in a bcc lattice. For a correct description of the multiple scattering process, it is necessary to assure that the muffin-tin spheres of adjacent atoms do not overlap. From the literature [13] oxygen phase shifts were taken which had been applied successfully in the LEED structural analyses of the systems Ni(110)–(2×1)–O [14] and Ru(0001)–$(\sqrt{3}\times\sqrt{3})$R 30°–Cs–O [5]. The phase shifts were temperature corrected using effective Debye temperatures of 420 K for Ru, 450 K for O and 150 K for Cs; the value for the Cs Debye temperature was chosen in a way that the corresponding mean-square deviation is consistent with the frequency of the Cs–Ru stretching vibration as provided by HREELS measurements [8]. The agreement between calculated and measured intensities was quantified by the r_{DE} factor [15] and by Pendry's r-factor r_P [16]. For the structural refinement, an automatic nonlinear least-squares optimization procedure with respect to r_{DE} [17] and r_P [18] was applied.

As demonstrated recently, the fingerprinting technique in LEED is often able to provide direct information on the local adsorption geometry [19]. In doing so, the experimental $I(E)$ curves of the half-order spots in the (2×2)–Cs and the $(2\sqrt{3}\times 2\sqrt{3})$R 30°–3Cs–2O phase were compared. They turned out to be very similar (see Fig. 1); the corresponding r_P-factor is 0.24. Because Cs is a much stronger scatterer than the lighter oxygen atom, these $I(E)$ curves contain information mainly about the local Cs adgeometry, i.e., about its adsorption site and height. From the structural analysis of the (2×2)–Cs structure it is known that the $I(E)$ curves are also affected by a buckling in the Ru substrate: in the Ru(0001)–(2×2)–Cs phase, the Ru atom below Cs is moved inwards by 0.1 Å. Therefore, it can be concluded tha the Cs adatoms in the $(2\sqrt{3}\times 2\sqrt{3})$R 30°–3Cs–2O structure sit near the on-top sites on a buckled Ru surface. Without this additional information, the structural analysis of this complex coadsorbate phase would have become too cumbersome and time consuming; note that apart from the 3Cs and 2O atoms at least the first ruthenium layer with 12 atoms has to be included as an

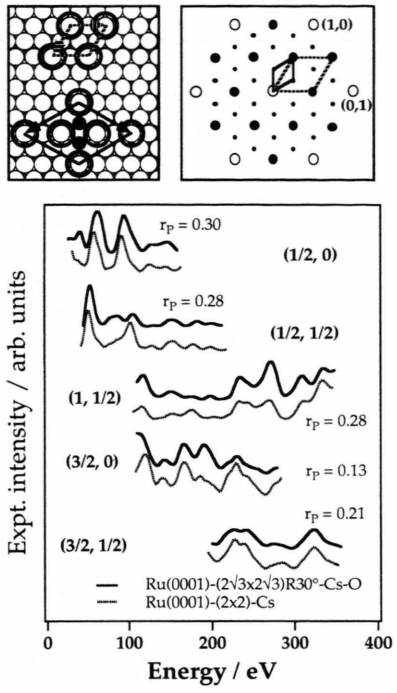

Fig. 1. a) Possible real space model (in comparison with the pure (2 × 2)–Cs structure) and schematic LEED pattern of the $(2\sqrt{3} \times 2\sqrt{3})$R 30° structure. The unit cells of the (2 × 2) structure (dotted lines) and of the $(2\sqrt{3} \times 2\sqrt{3})$R 30° structure (solid lines) are shown. Large circles: Cs atoms; small, solid circles: O atoms. b) Experimental $I(E)$ curves of the half-order beams of the pure Ru(0001)–(2 × 2)–Cs phase compared with those of the Ru(0001)–$(2\sqrt{3} \times 2\sqrt{3})$R 30°–3Cs–2O structure. The single beam r_P-factors are indicated; the overall r_P-factor between these experimental data sets is $r_P = 0.24$.

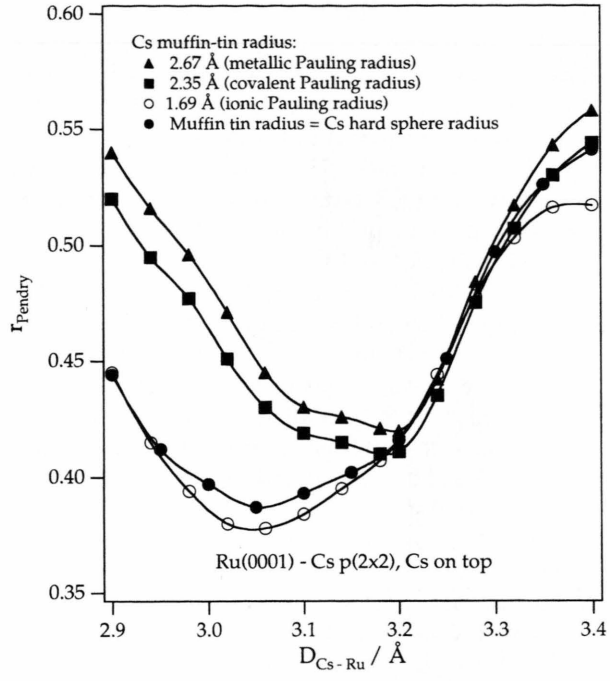

Fig. 2. r_P-factor as a function of the Cs–Ru interlayer spacing derived from calculations with Cs phase shifts computed with various muffin-tin radii.

additional overlayer in the analysis in order to take substrate relaxations into account.

In order to supply the structural analysis of the $(2\sqrt{3} \times 2\sqrt{3})$R 30°–3Cs–2O phase with an optimal set of Cs phase shifts, we performed some preliminary simulations with the Ru(0001)–(2 × 2)–Cs structure using phase shifts computed with various muffin-tin radii. This sophisticated treatment seems to be advisable because the Cs hard sphere radius can in principle take values ranging from the ionic (1.69 Å) to the metallic (2.67 Å) Pauling radius [20]. The (2 × 2)–Cs structure (instead of the complex $(2\sqrt{3} \times 2\sqrt{3})$R 30°–3Cs–2O structure) was chosen for convenience and the fact that the Cs adsorption geometry in both surfaces is very similar, as mentioned above. A data set containing 3 integer and 7 half-order beams measured at normal incidence at a temperature of 50 K was used for the comparison of theory with experiment. The r_P-factors as a function of the Cs–Ru interlayer distance for phase shifts calculated with muffin-tin radii corresponding to the ionic, covalent, and metallic Pauling radius [20] are collected in Fig. 2; the other parameters were kept fixed at their values of the optimum structure determined in a previous LEED analysis [6]. It can be seen that the phase shifts computed with ionic Cs radius improve the agreement between experiment and theory significantly and result in a shift of the optimum Cs–Ru spacing towards smaller values compared to calculations with covalent and metallic Cs radii. Also shown in Fig. 2 is the result of a calculation where the Cs muffin-tin radius and the Cs–Ru interlayer spacing are varied simultaneously. This means that the muffin-tin radius is always set to the Cs hard sphere radius, i.e., the Cs–Ru bond length minus the metallic radius of ruthenium of 1.35 Å, thus meeting the requirement of non-overlapping muffin-tin spheres of Cs and Ru. However, this analysis leads to nearly the same results as the calculations using the ionic muffin-tin radius. The phase shifts computed with the ionic muffin-tin radius were

therefore used for the structural analysis of the $(2\sqrt{3}\times 2\sqrt{3})$R 30°–3Cs–2O phase. A similar procedure was also applied to the Pt(111) system where decreasing the muffin-tin radius down to 0.95 Å led to a significant improvement of the *r*-factors [22].

In the structure analysis, we investigated all configurations where the oxygen atoms reside in threefold coordinated or in on-top sites with respect to the Ru(0001) substrate and Cs remain near on-top positions; the 5 possible models are depicted in Figure 3. In order to find suitable starting configurations for the automatic optimization procedure, in a first step, the O–Ru distance was varied over a wide range in parameter space for these configurations while all other parameters were kept fixed according to the optimum geometry found for the Ru(0001)–(2 × 2)–Cs structure [6]. In a second step, automatic refinements were performed with respect to r_{DE} as well as r_P including the vertical positions of the Cs and O adatoms, a buckling within the first substrate layer, and lateral displacements of the Cs adatoms consistent with the symmetry of the structures as indicated in Figure 3. The results compiled in Table 1 demonstrate that the agreement between theory and experiment is better for model 1

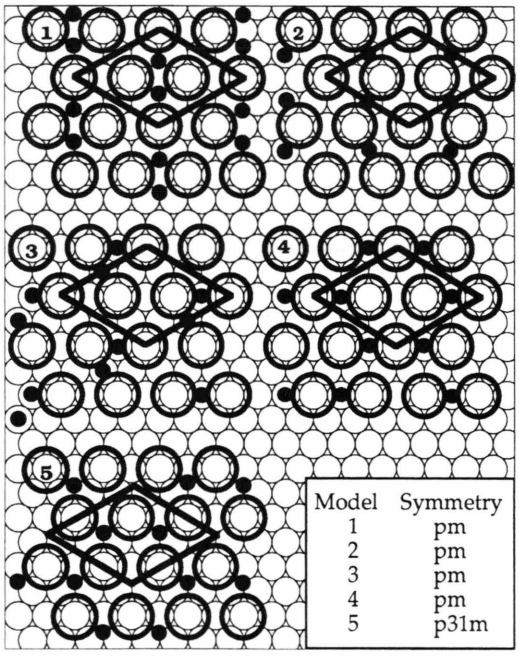

Fig. 3. Configurations of the Ru(0001)–$(2\sqrt{3}\times 2\sqrt{3})$R 30°–3Cs–2O structure considered in the LEED analysis. The symmetries are indicated (see inset). Large circles: Cs atoms; small filled circles: O atoms.

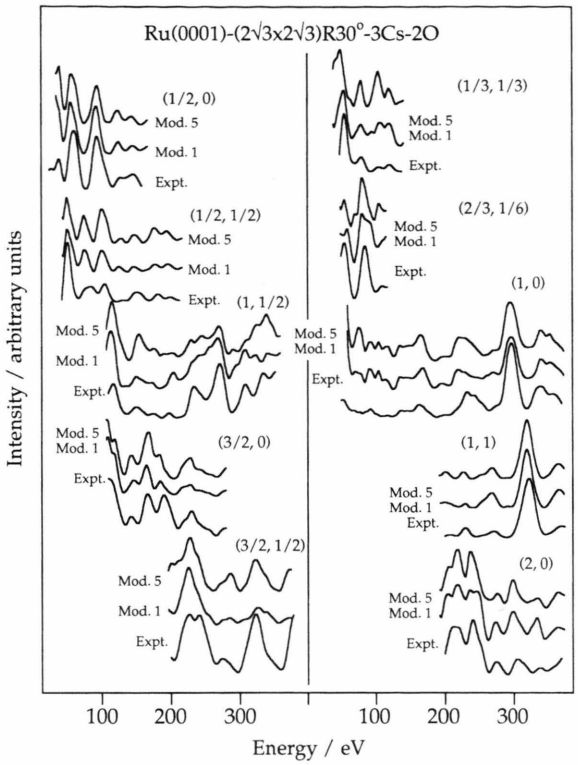

Fig. 4. $I(E)$ curves of model 1 and model 5 resulting from automated structural refinements in comparison with experiment.

Table 1. Interlayer spacings and *r*-factors for the optimized geometries of the models considered in the structural analysis.

Model	O adsite	D_{Cs-O}	D_{O-Ru}	r_{DE}	r_P
1	hcp/fcc	1.49 Å	1.46 Å	0.36	0.32
2	on top	0.96 Å	2.02 Å	0.39	0.40
3	on top	0.94 Å	2.05 Å	0.40	0.40
4	on top	0.91 Å	2.03 Å	0.40	0.43
5	hcp	1.51 Å	1.48 Å	0.35	0.32
5	fcc	1.50 Å	1.48 Å	0.39	0.40

and model 5 with oxygen in threefold coordinated sites than for the configurations with oxygen in on-top positions. The optimum *r*-factors for model 1 and model 5 are, however, nearly identical and do not allow to determine the lateral arrangement of the oxygen atoms; the corresponding $I(E)$ curves are displayed in Figure 4. In model 5, oxygen adatoms form a honeycomb structure with all oxygen atoms occupying either hcp sites or fcc sites; the configuration with

hcp sites reveals better *r*-factors. In model 1, oxygen occupies hcp as well as fcc positions.

Closer inspection of the optimum configurations of model 1 and model 5 reveals similarities of the local geometries of the Cs and the O adatoms, cf. Figure 5. Therefore, it is plausible that also the $I(E)$ curves and the *r*-factors are similar. A common structural element is the lateral shift of Cs adatoms away from the on-top sites reducing the Cs–O spacing. These displacements are presumably caused by interactions between Cs and O which are also reflected by the presence of the Cs–O vibration observed in HREELS [8]. In both configurations, the oxygen adatoms reside in threefold coordinated sites; like in the $(\sqrt{3}\times\sqrt{3})\mathrm{R}\,30°$ phase [5], oxygen is located below the plane of Cs cores. The hard sphere radii of Cs and O for the systems Ru(0001)–(2 × 2)–O, Ru(0001)–(2 × 2)–Cs and Ru(0001)–$(2\sqrt{3}\times 2\sqrt{3})\mathrm{R}\,30°$–3Cs–2O are compared in Table 2. It can be seen that the Ru–O bond length in the coadsorbate phase is about 0.1 Å longer than in the (2 × 2)–O structure which is indicative of a weakening of the Ru–O bond in the presence of coadsorbed Cs.

At oxygen coverages larger than 0.23, the $(2\sqrt{3}\times 2\sqrt{3})\mathrm{R}\,30°$ phase is replaced by an ordered $(\sqrt{39}\times\sqrt{39})\mathrm{R}\,16.1°$ structure [4]. Somewhat to our surprise, no Ru(0001)–(2 × 2)–Cs–O structure has been observed for a Cs:O stoichiometry of 1:1 which would represent the counterpart to the $(\sqrt{3}\times\sqrt{3})\mathrm{R}\,30°$–Cs–O coadsorption structure obtained with $\Theta_{Cs} = \Theta_O = 0.33$. Keeping this behavior in mind, we favor model 1; with model 5, adsorption of further oxygen in the free hcp sites would lead to a (2 × 2)–Cs–O structure in a very natural way. In model 1, the neighboring Cs adatoms are displaced from the on-top positions towards the oxygen, thus forming (2Cs + 2O) clusters, while the third Cs atom in the unit mesh stabilizes this structure. The Cs adatoms in the (2Cs + 2O) units are about 0.05 Å smaller than in the (2 × 2)–Cs structure; this value is, however, of the order of the error bars of the structure analysis. A similar behavior of the Cs and O radii was observed for the systems Ru(0001)–$(\sqrt{3}\times\sqrt{3})\mathrm{R}\,30°$–Cs and Ru(0001)–$(\sqrt{3}\times\sqrt{3})\mathrm{R}\,30°$–Cs–O and interpreted in terms of a charge transfer from Cs to oxygen [5]. The Cs–O distance in the (2Cs + 2O) units of (3.0 ± 0.1) Å is comparable with the corresponding spacing in the Cs peroxide which takes values between 2.95 Å and 3.05 Å [21].

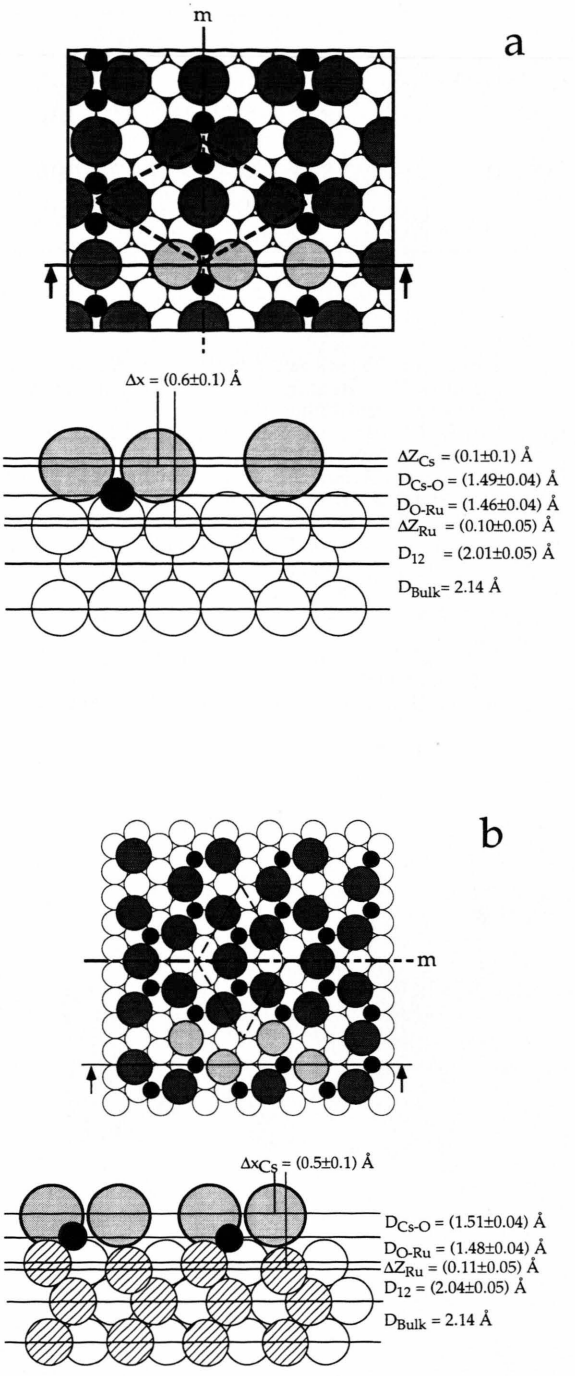

Fig. 5. Top view and magnified side view of the optimum geometries for the configurations with oxygen in threefold coordinated sites. Large, dotted circles: Cs atoms; small, filled circles: O atoms. The mirror plane (dash-dotted line) and the unit cell (dotted lines) are indicated. a) Model 1; b) model 5.

Table 2. Hard sphere radii of Cs and O for Cs–O coadsorbate structures in comparison with pure Cs phases and O phases on Ru(0001).

Structure	r_{Cs}/Å	r_O/Å	Ref.
Ru(0001)-(2×2)-Cs	1.80±0.07	–	[6]
Ru(0001)-$(2\sqrt{3}\times 2\sqrt{3})$R 30°-3Cs-2O model 1	1.75±0.07	0.79±0.05	this work
Ru(0001)-$(2\sqrt{3}\times 2\sqrt{3})$R 30°-3Cs-2O model 5	1.79±0.07	0.80±0.05	this work
Ru(0001)-(2×2)-O	–	0.68	[7]

[1] L. Surnev, in: Physics and Chemistry of Alkali Metal Adsorption, H. P. Bonzel, A. M. Bradshaw, and G. Ertl, Eds., Elsevier, Amsterdam 1989, pp. 173.
[2] G. Ertl, in: Catalytic Ammonia Synthesis, J. R. Jennings, Eds., Plenum, New York 1991.
[3] B. Woratschek, W. Sesselmann, J. Küppers, G. Ertl, and H. Haberland, J. Chem. Phys. **86,** 2411 (1989).
[4] H. Bludau, Ph.D. thesis, Freie Universität Berlin, 1992.
[5] H. Over, H. Bludau, M. Skottke-Klein, W. Moritz, and G. Ertl, Phys. Rev. B **46,** 4360 (1992).
[6] H. Over, H. Bludau, M. Skottke-Klein, G. Ertl, W. Moritz, and C. T. Campbell, Phys. Rev. B **45,** 8638 (1992).
[7] H. Pfnür, G. Held, M. Lindroos, and D. Menzel, Surf. Sci. **220,** 43 (1989).
[8] K. Jacobi, H. Shi, M. Gruyters, and G. Ertl, Phys. Rev. B **49,** 5733 (1994).
[9] H. Shi, Ph.D. thesis, Freie Universität Berlin, 1993.
[10] W. Moritz, J. Phys. C **17,** 353 (1984).
[11] R. Feder and W. Moritz, Surf. Sci. **77,** 505 (1978).
[12] K. Schwarz, Theor. Chimica Acta **34,** 225 (1974).
[13] S. Y. Tong, A. Macdonado, C. H. Li, and M. A. Van Hove, Surf. Sci. **94,** 73 (1980).
[14] G. Kleinle, J. Wintterlin, G. Ertl, R. J. Behm, F. Jona, and W. Moritz, Surf. Sci. **225,** 171 (1990).
[15] G. Kleinle, D. L. Adams, W. Moritz, and G. Ertl, Surf. Sci. **219,** L637 (1989).
[16] J. B. Pendry, J. Phys. C **13,** 937 (1980).
[17] G. Kleinle, W. Moritz, and G. Ertl, Surf. Sci. **238,** 119 (1990).
[18] M. Gierer, H. Over, and W. Moritz, unpublished.
[19] H. Over, M. Gierer, H. Bludau, G. Ertl, and S. Y. Tong, Surf. Sci. **314,** 243 (1994).
[20] L. Pauling, The Nature of the Chemical Bond, Cornell University Press, Ithaca, New York 1960.
[21] H. Föppl, Z. anorg. u. allg. Chemie **291,** 12 (1957).
[22] U. Starke, A. Barbieri, N. Materer, M. A. Van Hove, and G. A. Somorjai, Surf. Sci. **286,** 1 (1993).